

QC  
879  
5  
U47

*Susis analyzed*

NOAA Technical Report NESDIS 32



# Precipitation Detection with Satellite Microwave Data

Washington, D.C.  
June 1988

**U.S. DEPARTMENT OF COMMERCE**  
**National Oceanic and Atmospheric Administration**  
National Environmental Satellite, Data, and Information Service

NOAA TECHNICAL REPORTS  
National Environmental Satellite, Data, and Information Service

The National Environmental Satellite, Data, and Information Service (NESDIS) manages the Nation's civil Earth-observing satellite systems, as well as global national data bases for meteorology, oceanography, geophysics, and solar-terrestrial sciences. From these sources, it develops and disseminates environmental data and information products critical to the protection of life and property, national defense, the national economy, energy development and distribution, global food supplies, and the development of natural resources.

Publication in the NOAA Technical Report series does not preclude later publication in scientific journals in expanded or modified form. The NESDIS series of NOAA Technical Reports is a continuation of the former NESS and EDIS series of NOAA Technical Reports and the NESC and EDS series of Environmental Science Services Administration (ESSA) Technical Reports.

These reports are available from the National Technical Information Service (NTIS), U.S. Department of Commerce, Sills Bldg., 5285 Port Royal Road, Springfield, VA 22161 (prices on request for paper copies or microfiche, please refer to PB number when ordering) or by contacting Nancy Everson, NOAA/NESDIS, 5200 Auth Road, Washington, DC 20233 (when extra copies are available). A partial listing of more recent reports appear below:

NESDIS SERIES

- NESDIS 1 Satellite Observations on Variations in Southern Hemisphere Snow Cover. Kenneth F. Dewey and Richard Heim, Jr., June 1983. (PB83 252908)
- NESDIS 2 NODC 1 An Environmental Guide to Ocean Thermal Energy Conversion (OTEC) Operations in the Gulf of Mexico. National Oceanographic Data Center, June 1983. (PB84 115146)
- NESDIS 3 Determination of the Planetary Radiation Budget from TIROS-N Satellites. Arnold Gruber, Irwin Ruff and Charles Earnest, August 1983. (PB84 100916)
- NESDIS 4 Some Applications of Satellite Radiation Observations to Climate Studies. T.S. Chen, George Ohring and Haim Ganot, September 1983. (PB84 108109)
- NESDIS 5 A Statistical Technique for Forecasting Severe Weather from Vertical Soundings by Satellite and Radiosonde. David L. Keller and William L. Smith, June 1983. (PB84 114099)
- NESDIS 6 Spatial and Temporal Distribution of Northern Hemisphere Snow Cover. Burt J. Morse and Chester F. Ropelewski (NWS), October 1983. (PB84 118348)
- NESDIS 7 Fire Detection Using the NOAA--Series Satellites. Michael Matson, Stanley R. Schneider, Billie Aldridge and Barry Satchwell (NWS), January 1984. (PB84 176890)
- NESDIS 8 Monitoring of Long Waves in the Eastern Equatorial Pacific 1981-83 Using Satellite Multi-Channel Sea Surface Temperature Charts. Richard Legeckis and William Pichel, April 1984. (PB84 190487)
- NESDIS 9 The NESDIS-SEL Lear Aircraft Instruments and Data Recording System. Gilbert R. Smith, Kenneth O. Hayes, John S. Knoll and Robert S. Koyanagi, June 1984. (PB84 219674)
- NESDIS 10 Atlas of Reflectance Patterns for Uniform Earth and Cloud Surfaces (NIMBUS-7 ERB--61 Days). V.R. Taylor and L.L. Stowe, July 1984. (PB85 12440)
- NESDIS 11 Tropical Cyclone Intensity Analysis Using Satellite Data. Vernon F. Dvorak, September 1984. PB85 112951)
- NESDIS 12 Utilization of the Polar Platform of NASA's Space Station Program for Operational Earth Observations. John H. McElroy and Stanley R. Schneider, September 1984. (PB85 1525027AS)
- NESDIS 13 Summary and Analyses of the NOAA N-ROSS/ERS-1 Environmental Data Development Activity. John W. Sherman III, February 1984. (PB85 222743/43)
- NESDIS 14 NOAA N-ROSS/ERS-1 Environmental Data Development (NNEEDD) Activity. John W. Sherman III, February 1985. (PB86 139284 A/S)
- NESDIS 15 NOAA N-ROSS/ERS-1 Environmental Data Development (NNEEDD) Products and Services. Franklin E. Kniskern, February 1985, (PB86 213527/AS)

QC  
879.5  
.U47  
no. 3h



## NOAA Technical Report NESDIS 32

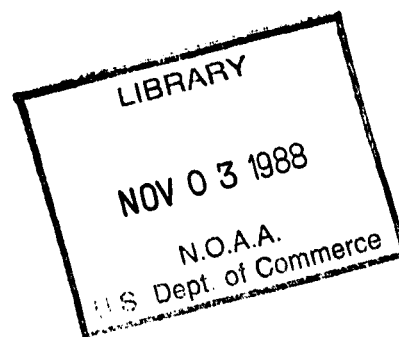
# Precipitation Detection with Satellite Microwave Data

Yang Chenggang  
Institute of Agrometeorology  
Academy of Meteorological Science  
State Meteorological Administration  
Beijing, People's Republic of China

and

Andrew Timchalk  
Satellite Applications Laboratory  
Washington, D.C.

June 1988



**U.S. DEPARTMENT OF COMMERCE**

C. William Verity, Secretary

**National Oceanic and Atmospheric Administration**

William E. Evans, Under Secretary

National Environmental Satellite, Data, and Information Service

Thomas N. Pyke, Jr., Assistant Administrator

# **National Oceanic and Atmospheric Administration TIROS Satellites and Satellite Meteorology**

## **ERRATA NOTICE**

One or more conditions of the original document may affect the quality of the image, such as:

Discolored pages  
Faded or light ink  
Binding intrudes into the text

This has been a co-operative project between the NOAA Central Library and the Climate Database Modernization Program, National Climate Data Center (NCDC). To view the original document contact the NOAA Central Library in Silver Spring, MD at (301) 713-2607 x124 or [Library.Reference@noaa.gov](mailto:Library.Reference@noaa.gov).

HOV Services  
Imaging Contractor  
12200 Kiln Court  
Beltsville, MD 20704-1387  
January 26, 2009



## CONTENTS

	<u>Page</u>
List of Figures.....	iv
List of Tables.....	v
ABSTRACT.....	1
I. INTRODUCTION.....	2
II. PROCEDURE AND DATA USED.....	3
III. RESULTS.....	5
3.1 Screening regression of effective rain rate (ERR) against all MSU channels.....	5
3.2 Relationship between effective rain rate (ERR) and the median filter anomaly of MSU Ch 2 (MFA2).....	7
3.3 Relationship between effective rain rate (ERR) and MSU Ch 2 brightness temperature (TB2).....	9
IV. SUMMARY.....	10
V. ACKNOWLEDGEMENTS.....	11
VI. REFERENCES.....	12

## LIST OF FIGURES

<u>Figure</u>	<u>Page</u>
1. Temperature weighting functions for the four MSU channels for nadir and beam positions #1 and #11 (0=56.6 deg). Weighting functions are shown for land ( $\epsilon=1$ ) and sea ( $\epsilon=0.5$ ) type surfaces.....	13
2. Example of MSU2 brightness temperature (TB2) array used to calculate the median filter anomaly (MFA2).....	14
3a. MSU footprints (IFOV) for 0056 GMT April 8, 1986 .....	15
3b. Radar echo summary chart for 0035 GMT April 8, 1986 .....	15
3c. GOES 6 infrared image 0100 GMT April 8, 1986.....	16
3d. Six hourly precipitation 06 GMT April 8, 1986.....	16
4. Correlation of Effective Rain Rate (ERR) with MSU variables for 0056 GMT Apr 8, 1986. Abscissa shows order of variable selection using forward stepwise regression method.....	17
5. Same as Figure 4 except for 1245 GMT July 1, 1986.....	18
6. Same as Figure 4 except for 1317 GMT October 24, 1986.....	19
7. Same as Figure 4 except for 2005 GMT December 9, 1986.....	20
8. Same as Figure 4 except for April 8, July 1, and October 24, 1986 cases combined (over land only) .....	21

## LIST OF TABLES

<u>Table</u>	<u>Page</u>
1. Radar-echo level (VIP number) conversion to rain rates.....	22
2. Screening regression statistics for ERR as a function of all four MSU TB and MFA values (land only).....	22
3. Effective Rain Rate (ERR) regressed on Median Filter Anomaly of MSU Ch 2 (MFA2).....	23
4. Effective Rain Rate (ERR) regressed on MSU Ch 2 (TB2).....	23
5. Distribution of Ch 2 Median Filter Anomaly (MFA2) as a function of Effective Rain Rate (ERR) for 0056 GMT April 8, 1986.....	24
6. Distribution of Ch 2 Median Filter Anomaly (MFA2) as a function of Effective Rain Rate (ERR) for 1245 GMT July 1, 1986.....	24
7. Distribution of Ch 2 Median Filter Anomaly (MFA2) as a function of Effective Rain Rate (ERR) for 1317 GMT October 24, 1986.....	25
8. Distribution of Ch 2 Median Filter Anomaly (MFA2) as a function of Effective Rain Rate (ERR) for 2005 GMT December 5, 1986.....	25
9. Distribution of Ch 2 Median Filter Anomaly (MFA2) as a function of Effective Rain Rate (ERR) for April, July, and October, 1986 cases combined.....	26
10. Distribution of Ch 2 Median Filter Anomaly (MFA2) as a function of Effective Rain Rate (ERR) for April, July, October, and December, 1986 cases combined.....	26
11. Effective Rain Rate (ERR) values regressed on Ch 2 Median Filter Anomaly (MFA2) values for each ERR class. Samples are for April, July, and October, 1986.....	27

## PRECIPITATION DETECTION WITH SATELLITE MICROWAVE DATA

Yang Chenggang  
Institute of Agrometeorology  
Academy of Meteorological Science  
State Meteorological Administration  
Beijing, People's Republic of China

and

Andrew Timchalk  
Satellite Applications Laboratory  
Washington, DC

**ABSTRACT.** When all four channels of the NOAA polar-orbiting satellite Microwave Sounding Unit (MSU) instrument were screened against a measure of rainrate, MSU Ch 2 (53.74 Ghz) was found to be the most useful channel for detecting precipitation over land. A median filter algorithm which isolates the decrease in brightness temperature of MSU Ch 2 from the normal background temperature in this channel was used to calculate a Median Filter Anomaly (MFA2).

The MFA2 values were found to be correlated with an Effective Rain Rates (ERR). Coefficients were as high as 0.6 over land during the spring and summer cases. Correlation was highest when convection was strong and echo tops reached to near the tropopause levels.

In the winter cases, convection was relatively weak and rain rates were small. Echo tops were relatively low and reached to only approximately 25,000 ft. For the winter cases, the MFA2 algorithm showed no skill in detecting precipitation.

Results indicate that the MFA2 is marginally useful in detecting rain rates. Its operational use in the TIROS Operational Vertical Sounding (TOVS) algorithm, however, does serve well to prevent "cold" biased temperature retrievals from being calculated in areas where precipitation contamination is strong.

## I. INTRODUCTION

Prior to 1979, polar-orbiting satellite temperature retrievals were used experimentally. Beginning in 1979, satellite temperature profiles were produced routinely by the National Environmental Satellite, Data, and Information Service (NESDIS) and used operationally by the National Meteorological Center (NMC).

By 1980, it was found that cloudy path temperature retrievals made with the microwave channels showed a lower (cold) temperature bias when heavy precipitation rates were reported (Phillips, 1980; Hubert et al., 1981). Subsequently, tests were devised to prevent retrievals from being calculated if precipitation was suspected to be biasing the MSU brightness temperature measurements and thereby biasing the retrieved temperatures.

These early tests were devised for oceanic areas, where the water surface emissivity is more uniform and about one-half of that over land surfaces. These two factors make the MSU window Ch 1 (50.73 GHz) much more sensitive to clouds and precipitation over water. Over land, however, MSU Ch 1 cannot be used in the precipitation tests simply because it is too sensitive to the large variations of surface emissivity typically found over land areas.

At the present time, quantitative estimates of rainfall are made operationally based upon a satellite data technique developed by Scofield (1987), Scofield and Oliver (1977). This technique relies heavily upon the vertical extent of the convective cloud tops that are determined from satellite infrared imagery. Various techniques for estimating rainfall have been developed by Griffith et al. (1978), Negri and Adler (1987), Arkin (1979), and others. These techniques are based primarily on the use of infrared or infrared and visible satellite data. Barrett's technique (1981) includes cloud types as well as climatological constraints.

Studies by Staelin et al. (1975) pertaining to the SCanning Microwave System (SCAMS) instrument indicated that microwave temperature retrievals should not be affected by clouds with less than 0.01 gm/cm<sup>2</sup> liquid water.

Numerous authors have reported on the use of passive microwave measurements to detect precipitation. It was concluded by Atlas (1981) that passive microwave radiometry will become useful over the oceans with the advent of higher resolution, but that useful measurements over land are much less promising.

Grody (1983) showed no effects due to precipitation in the MSU channels for radar intensities of less than level-3, which is a radar estimate of less than 41.9 mm/hr (Table 1), when he examined microwave measurements over a convective storm of 12 April 1979 over the central United States.

Studies of rain rates with Scanning Multichannel Microwave Radiometer (SMMR) data by Spencer (1984, 1985a) have shown correlations as high as 0.80 over land in the summer.

A recent paper discussing the precipitation effects on Microwave Sounding Unit (MSU) data by Nappi et al. (1986) provided the stimulus for this study. In that study, a median filter algorithm was devised to detect and eliminate precipitation contamination in the operational MSU retrieval procedure.

The main purpose of our study was to evaluate the sensitivity of MSU channels in detecting precipitation over land, namely, over the United States. All four MSU channel brightness temperatures (TB's) plus all four derived Median Filter Anomaly (MFA) values were statistically screened for possible useful relationships with precipitation.

In addition, a large part of our work concentrated on the evaluation of the precipitation-induced decreases of MSU Ch 2 brightness temperatures (TB2) discussed by Grody (1982, 1983) and the sensitivity of a Median Filter Algorithm (MFA) in detecting precipitation.

The main question addressed was: How well does the Median Filter Anomaly of MSU Ch 2 (MFA2) detect precipitation areas and intensities over land?

## II. PROCEDURE AND DATA USED

MSU brightness temperatures (TBs) were obtained from the NOAA 6 and 9 polar orbiting satellites for the period, April through December 1986. The data were collected directly from the operational files with the assistance of the NESDIS Sounding Implementation Branch and the ST Systems Corporation Technologies personnel. Data were extracted from the files at the point where the raw MSU TB's had been earth located, limb corrected, and calibration corrected, but before any of the MSU channels were flagged for elevation or precipitation contamination.

MSU TB's are flagged for several reasons. For example, MSU Ch 2 TB is flagged if surface terrain elevation is high enough to affect the channel measurement. Figure 1 shows the weighting functions for the four MSU channels. Even though the weighting function of MSU Ch 2 (53.74 GHz) peaks near 600 mb, the area within the lower limb of the weighting function increases rapidly with elevation. Thus the brightness temperature of Ch 2 (TB2) is significantly affected when the surface elevation reaches higher than about 1500 meters (850 mb). When this occurs in the operational procedure, the MSU TB2 values are flagged and TB2 is not used to generate a retrieval at that location.

The Median Filter Anomaly (MFAx) was calculated separately for all four MSU Channels (1,2,3,4). An example of how the MFA is calculated is shown in

Figure 2. In this example, Ch 2 brightness temperatures (TB2) were used to derive MFA2. The MFA2 is derived by using a moving 3 x 3 array of MSU Ch x brightness temperatures (TBx) to filter out possible precipitation contamination at the center position of the array. The MFA2 is defined as the difference between the median TBx value and the central TBx value. In Figure 2, the median TB2 value of the nine points is 253°K. The central value is 251°K. Thus, the MFA2 value is equal to a positive 2.0°K. Precipitation is suspected if the MFA2 value is larger than 1.0°K.

In the current operational procedure, if the MFA2 exceeds 0.8°K then the rain test failure is invoked, the MSU TB2 is set to zero, and no retrieval is calculated for that particular point.

Because the instantaneous field of view (IFOV) of the MSU instrument is quite large, several methods were considered in order to obtain a representative measure rain area and/or rain rate. Figure 3a illustrates the eleven beam positions and the earth-located IFOVs of the MSU channels for the April 8, 1986 case. At the nadir beam #6 position, the resolution is about 110 km, while at the outer beam positions (#1 and #11), the footprint shape is elliptical with axes of 323 km and 179 km.

To obtain rain rates, we used the NMC Radar Summary charts and the Z-R relationship for convective precipitation (Table 1) developed by the National Weather Service, (Hallgren 1979). Rain rates were determined at each MSU beam position by first overlaying the MSU footprints atop the Radar Summary charts. We then estimated the areal coverage of each radar echo intensity level within each of the MSU footprints. These areally-weighted echo intensities were then converted to an Effective Rain Rate (ERR mm/hr) by using the weighting shown in Equation (1).

$$ERR = \sum A_i R_i \quad \text{Eq. (1)}$$

In Equation (1),  $A_i$  is the percentage area of radar-echo intensity within the MSU footprint and  $R_i$  is the rain rate prescribed by each VIP level as given in Table 1. On the radar-echo charts, echo levels 1, 3, and 5 are mapped out as shown in Figure 3b.

Figures 3c and 3d show the corresponding GOES 6 infrared image and six hourly precipitation charts, respectively. These two figures will be discussed later in Section 3.2.

Although other cases were extracted and examined, we restricted our detailed statistical analyses to a representative sample. The cases presented here will include 0056Z April 8, 1245Z July 1, 1317Z October 24, and 2005Z December 9, 1986.

### III. RESULTS

#### 3.1 Screening Regression of Effective Rain Rate (ERR) Against All MSU Channels

As our first step, we used as independent variables, the brightness temperatures (TB) of four MSU channels represented by (B<sub>1</sub>-B<sub>4</sub>) and the median filter anomalies (MFA) of the four channels represented by (B<sub>5</sub>-B<sub>8</sub>), as shown in Table 2. These eight variables were statistically screened to search for a useful relationship with the ERR values. A Forward Stepwise Screening Regression program was run separately for each of four days: April 8, July 1, October 24, and December 9, 1986 and for the first three dates combined. Besides partitioning the data by date, the data were also partitioned into sets over land only, and rain only sets, as shown in Figures 4 through 8.

Table 2 shows a tabulation of the screening statistics for each of the above dates. The statistics are assumed to represent the conditions during spring, summer, fall, and winter.

Points over the ocean and the Great Lakes were included in Figures 4 through 7 above, but the results over water areas will not be presented hereafter since the sample sizes over water were quite small. Small sample sizes over ocean areas result because the radar coverage was available at only a few coastal radar sites. Table 2 shows the statistics over land only for each date (season) and the first three orbits/dates (seasons) combined. The three orbit combination exclude the winter case. Each date (season) is shown subdivided into two ERR classes: (1) Rain + No Rain represented by (R + NR), and (2) Rain only represented by (R).

Values under column (R + NR) include all available points. These include points for which Rain and No Rain was determined via the radar charts; while the column labelled R shows only points for which rain was determined. The sample size is given in row n. In the long regression equation shown near the bottom of Table 2, B<sub>0</sub> is the intercept and B<sub>1</sub> through B<sub>4</sub> are the coefficients for the MSU TB<sub>1</sub> through TB<sub>4</sub> variables respectively; while, B<sub>5</sub> through B<sub>8</sub> are the corresponding coefficients for the MSU MFA<sub>1</sub> through MFA<sub>4</sub> variables. The regression coefficient is denoted by "r", the Standard Error by "S". ERR(AV) is the average effective rain rate in mm/hr, and TB<sub>2</sub>(AV) is the average brightness temperature (°K) of MSU Ch 2.

If an "X" is tabulated in lieu of any of the independent variable coefficients, that particular variable was not chosen during the screening run. It therefore contained little or no relationship to the effective rain rate (ERR).

By examining the screening results, we found that the independent variables, MFA2 and TB2, contained practically all of the rain rate information. At this juncture, we turned our attention toward examining the Median Filter Anomaly algorithm. Our results corroborate those of Grody (1982) and Nappi et al. (1986), showing that MSU Channel 2 (53.74 GHz) is the most sensitive of the four MSU channels for precipitation detection. Of the four MSU channels, our data set showed that Channel 3 (54.96 GHz) was the least sensitive to precipitation.

The December 9 case was subsequently isolated from the combined set because the most frequently chosen variable, MFA2 (B6), was not selected for that case. In Table 2, those variables, whose coefficients are labelled X, contributed an insignificant amount of explained ERR variance and thus their non-selection is simply the result of arbitrarily setting the limiting F statistic to 0.5.

Figures 4 through 8 show the order in which the independent variables were selected and the corresponding improvement in the correlation coefficient ( $r$ ) as more variables are added by the screening process.

In Figures 4 through 7, parts (a) and (b) include the sample points over both land and water surfaces, while parts (c) and (d) include sample points over land only. Parts (b) and (d) of these figures are restricted to those sample points over which the Effective Rain Rate (ERR) was  $>0$ , i.e., points at which rain ( $R$ ) was occurring (as determined from the radar charts). Parts (a) and (c), however, included all sample points whether or not rain was occurring ( $R + NR$ ). The screenings show that the MFA2 variable was selected first in most runs.

In Figure 4, April 8, 1986, the MFA2 variable was selected first in parts (a), (b), and (d), while MFA1 was selected first in part (c) with MFA2 second. Since part (c) contained points over land only, we suspect that the MFA1 selection was due to a strong reduction of surface emissivity caused by wet land areas where rain had recently fallen.

In Figure 5, July 1, 1986, MFA2 was selected first in all four partitions. The selection of the second variable was mixed.

In Figure 6, October 24, 1986, MFA2 was selected first in only part (c). MFA1 was selected first in parts (b) and (d) and TB2 was selected first in part (a). Note that TB2 was the second selection in parts (c) and (d).

In Figure 7, December 9, 1986, MFA2 was not selected in any of the parts. TB2 was selected first in all four parts. Recall that a variable may not be selected simply because the screening was halted when the F statistic reached 0.5. The selection of TB2 in this winter case was not surprising but a positive correlation was unexpected.

Figure 8 shows the April 8, July 1, and October 24, 1986 cases combined. Only the cases over the land are shown. The MFA2 was selected first and explained nearly all of the variance of the Effective Rain Rate (ERR). In the 302 cases of the (R + NR) class, the cumulative correlation coefficient was 0.56. This compares to the 0.67 value of the 94 cases of the Rain only (R) class. Hence, the explained variance was 45% for the R class and 31% for the (R + NR) class.

As seen later in Table 4, a sign reversal in the correlation between ERR and TB2 occurred in both the October and December cases. The sign reversal is particularly significant in the December case since it reveals a weakness inherent in the present MFA2 algorithm. This weakness will be discussed later in Section 3.3.

### 3.2 Relationship Between Effective Rain Rate (ERR) and the Median Filter Anomaly (MFA2)

Table 3 shows the results of the ERR values regressed on the MFA2 values. The highest correlations of 0.66 and 0.67 were found in the April and July cases when rain was occurring (R). For these dates, if non-raining points are combined with the raining points (R + NR), then the correlations are reduced to 0.58 and 0.57, respectively.

Thus if the points over land for the spring and summer cases are considered, we see that the MFA2 algorithm explained more than 43% ( $r^2$ ) of the ERR variance when rain was occurring. But, the explained ERR variance was reduced to about 32% when non-raining points were included. This finding indicates that the MFA2 algorithm is more sensitive when rain is observed and that the algorithm does contain some false alarm potential; i.e., the MFA2 values exceeded the  $1.0^\circ\text{C}$  threshold value, indicating precipitation, when in fact none was observed. Overall, we see that for the spring and summer cases, at least 32% of the rain rate information was accounted for by the MFA2 values.

In the October 24, 1986 (fall) case, the correlations were lower than in the spring and summer cases. Correlations were 0.42 and 0.32 for the rain only (R) and the rain plus no rain (R + NR) classes respectively. Thus, only about 18% and 10% of the ERR variance of their respective classes could be explained by the MFA2 values.

In the December 9, 1986 (winter) case, the correlation between the ERR and MFA2 was further reduced. The positive relationship, in the first three dates (seasons), disappeared totally and a small negative relationship is indicated. The actual  $r$  values were -0.12 and -0.04, respectively.

Tables 5 through 10 show the distribution of MFA2 values as a function of ERR for each date separately and in combined sets. Here, the ERR values are divided into four standard National Weather Service (NWS) rain rate

categories: HEAVY, MODERATE, LIGHT, and NO RAIN. HEAVY was defined as ERR greater than 7.62 mm/hr, MODERATE as 2.54 to 7.62 mm/hr, and LIGHT as less than 2.54 mm/hr. NO RAIN was assigned to points where no echoes were plotted on the radar charts within the MSU footprint.

In Table 5, of the 81 footprints (points) for which data was analyzed on April 8, radar charts indicated rain was falling at 18 points (22%) while no rain was indicated at 63 of the points (78%). Of the 18 rain cases, 4 of the 5 points in the MODERATE and HEAVY classes showed MFA2 values greater than 1.5°K or larger; while in the LIGHT rain category 5 of the 13 points showed negative MFA2 values. In the NO RAIN category, the MFA2 values were generally negative. However, two points in this category had MFA2 values larger than 1°K.

The point marked by the "#" symbol (MFA2=1.7K) was located at 34.9N 112W and was related to an unflagged surface elevation over the Colorado Plateau in Arizona. At least 30% of this footprint was located over elevations above 1800 meters. The point marked by the "\*" symbol (MFA = 1.3K) was located at 31.8N 89.6W over northern Mississippi. There was no elevation problem here, but we suspect that falling rain or clouds containing large liquid water drops were associated with this point although it was not indicated by the radar echo charts.

We note that the New Orleans radar was out for maintenance at this time. The six hourly synoptic precipitation chart (see Figure 3d) showed no measurable precipitation over the reporting stations in Mississippi; however, the GOES 6 cloud picture (Figure 3c) showed an elongated overcast cold-cloud-top over that area. Given these conditions, we suspect that the 1.3K MFA2 value was caused by precipitation that fell between reporting stations.

An analyses of the the rain rates and the vertical extent of the radar summary chart echo-tops indicate that the MFA2 algorithm is most sensitive to precipitation when the rain rates are large and the echo-tops reach to tropopause heights. These conditions occur most frequently in the spring and summer over the United States when convection is most pronounced and rain rates are very high.

The seasonal effect is clearly seen in Table 2. In the December case, the effective rain rate averaged only 2.89 mm/hr compared to 7.96 mm/hr for the April case. Thus, the April ERR was 2.75 times larger than the December ERR. Echo-tops reached as high as 56,000 feet in the April case compared to only about 20,000 feet over New York State (28,000 feet over northern Alabama) in the December case (not shown).

Finally, we found that the relationship between ERR and MFA2 was better over land than over land and water areas combined. A probable reason is

that large land-water temperature gradients (land-sea breeze thermal structures) exist along coast lines and if these temperature gradients are sufficiently strong and deep enough, they influence the TB2 values and thence the MFA2 values.

Further, we see that the relationship is better for the rain class than for the no rain plus rain class. This relationship results because the brightness temperatures of Ch 2 (TB2) includes emission from the warmer near-surface boundary layer in the relatively clear skies of the no rain areas; but, in the rain areas, the Ch 2 brightness temperatures (TB2) are reduced by rain-scattering coupled with the suppression of emission from the warmer near-surface boundary layer.

The correlation between ERR and MFA2 changed with rain rate. Table 11, shows that the correlation with MFA2 increased as rain rates increased. The MFA2 is more likely to detect moderate and heavy rain, (i.e., ERR greater than 2.54 mm/hr); while, it shows no ability ( $r=-0.04$ ) to detect light rain, (i.e., ERR less than 2.54 mm/hr). The correlation coefficients were .30 and .45 for moderate and heavy effective rain rates, respectively.

### 3.3 Relationship Between Effective Rain Rate (ERR) and MSU Ch 2 Brightness Temperature (TB2)

As seen in the screening regressions of Figures 4 through 8, TB2 was not selected as an important variable in its relationship to ERR on either April 8 or July 1 dates. Results were mixed for the October 24 date, while TB2 was the first variable selected on the December 9 date. On individual cases over land, it was expected that TB2 would show markedly lower values under heavy rain conditions. However, it is clear from this study that the relationship between ERR and absolute values of TB2 is poor.

The correlations however, became positive on the October 24 and December 9 dates reaching as high as 0.42. The switch in the sign of the correlation coefficients indicates that the absolute values of the Ch 2 temperature themselves (TB2) cannot be used to estimate precipitation and further, that the important factor is the relative decrease of TB2.

Table 4 shows the results of the ERR values regressed on the TB2 values. The highest correlation ( $r=-0.47$ ) occurred on the April 8 date, for those footprints at which Rain was falling (R). The correlation was very low (-0.06 and -0.15) but still negative on the July 1 date.

Table 4 also shows, as did Table 3, that ERR value was 7.96 mm/hr for the April 8 date and 2.89 mm/hr for the December 9 date. However, note that the correlation for the first three dates (3 orbits) was near zero (-0.08). This indicates that the absolute values of TB2 themselves cannot be used to determine rain areas or rain rates.

By using data from the April 8 case, it was found that about 64% ( $r=-0.8$ ) of the variance of TB2 was explained by its latitudinal gradient. Between latitudes 30N-50N, the TB2 decreased by about 0.5 K/deg latitude. When this latitudinal gradient was removed from the TB2 field and the MFA2 then applied, there was no significant improvement in the MFA2-ERR relationship. This indicates an important feature of the three-row matrix of the MFA algorithm, i.e., the northernmost (colder) row is largely compensated for by the southernmost (warmer) row.

Thus, the MFA algorithm demonstrates that it is the areal anomaly of TB2 that is important. To be successful in detecting precipitation with this channel, any approach must be designed such that the anomaly (decrease in TB2) caused by precipitation is isolated from the existing background thermal emission. For the cases examined in this study, the MFA2 (3 x 3) filter served well to isolate decreases of TB2 caused by moderate or heavy precipitation.

#### IV. SUMMARY

Of the four MSU channels, channel 2 (53.74 GHz) was the most useful channel in detecting precipitation over land. The brightness temperature values (TB2) of channel 2 alone were not sufficient to detect precipitation; but, a median filter algorithm (MFA2), which isolates precipitation induced decreases in TB2 from the normal background radiative temperature, showed the highest correlations with effective rainfall rate.

The MFA2 value was correlated with Effective Rainfall Rate (ERR) with correlation coefficients of about 0.6 during the spring and summer cases; but during the winter, correlations were near zero.

This study concludes that precipitation is more easily detected over land, with the use of the 53.74 GHz channel 2 via the MFA2 algorithm, during spring and summer when convection is strong (reaching to tropopause levels) and when rain rates are high.

Because of the vertically broad weighting function of MSU Ch 2, which peaks at about the 600 mb level, the MFA2 algorithm should not be used over mountainous areas where heights are above 1500 meters. The 1500-meter elevation flag is currently in use and has been utilized in the TOVS algorithm since 1980.

The present MSU instrument with its low resolution shows no skill in detecting rain rates when they are light. In addition, the algorithm is not reliable when surface elevations exceed 1500 meters; further, it should not be used for those footprints over coastal areas where strong land-water thermal gradients (seabreeze circulations) are suspected to extend higher than one km into the lower atmosphere.

In the current operational procedure, the rain test failure is invoked and no retrieval is calculated for a particular point if the MFA2 value exceeds 0.8°K. As shown in Table 10, when the MFA2 values were greater than 1.0°K, they were clustered in the heavy and moderate ERR classes.

Over non-mountainous land areas, the statistics show that when the MFA2 was positive and 1.0°K or greater, the ERR was greater than 2.54 mm/hr. If the MFA2 was negative and less than -0.5°K, then there was at least a 93% chance that the ERR was less than 2.54 mm/hr or that no rain was occurring.

Although the MFA2 algorithm is marginally useful in deriving rain rates, it does serve well to prevent cold-biased satellite temperature retrievals from being calculated at those points where moderate or heavy precipitation is occurring.

Finally, with the higher resolution and dual polarizations of the SSMI (Special Sensor Microwave Imager) and AMSU (Advanced Microwave Sounding Unit), it is anticipated that algorithms can be devised to better detect rain rates and their areal extent.

#### V. ACKNOWLEDGEMENTS

We wish to thank the Sounding Implementation Branch and ST Systems Corporation members for their support in obtaining the MSU data used in this study. In particular, we thank A. Nappi for his assistance in obtaining the MSU Median Filter Anomaly values from the operation files.

Thanks also to members of the Satellite Applications Laboratory for their support and consultation. Thanks to J. Shadid for help on the figures, T. Cashman for final typing, and to F. Holt and N. Grody for editorial review.

#### VI. REFERENCES

- Arkin, P.A., 1979: The relationship between fractional coverage of high cloud and rainfall accumulations during GATE over the B-scale array. Mon. Wea. Rev., 107, 1382-1387.
- Atlas, D., 1981: Precipitation measurements from space. NASA Workshop Report, October, David Atlas and Otto W. Thiele (Eds.), p. D-351.
- Barrett, E.C. and D.W. Martin, 1981: The use of satellite data in rainfall monitoring. Academic Press, New York, NY, 340 pp.
- Griffith C.G., W.L. Woodley, P.G. Grube, D.W. Martin, J. Stout, and D. Sikdar, 1978: Rain estimation from geosynchronous satellite imagery: Visible and infrared studies. Mon. Wea. Rev., 106, 1153-1171.
- Grody, N.C. and W.C. Shen, 1982: Observations of hurricane David (1979) using the microwave sounding unit. NOAA Technical Report NESS 88, Dept. of Commerce, Washington, DC.

By using data from the April 8 case, it was found that about 64% ( $r=-0.8$ ) of the variance of TB2 was explained by its latitudinal gradient. Between latitudes 30N-50N, the TB2 decreased by about 0.5 K/deg latitude. When this latitudinal gradient was removed from the TB2 field and the MFA2 then applied, there was no significant improvement in the MFA2-ERR relationship. This indicates an important feature of the three-row matrix of the MFA algorithm, i.e., the northernmost (colder) row is largely compensated for by the southernmost (warmer) row.

Thus, the MFA algorithm demonstrates that it is the areal anomaly of TB2 that is important. To be successful in detecting precipitation with this channel, any approach must be designed such that the anomaly (decrease in TB2) caused by precipitation is isolated from the existing background thermal emission. For the cases examined in this study, the MFA2 (3 x 3) filter served well to isolate decreases of TB2 caused by moderate or heavy precipitation.

#### IV. SUMMARY

Of the four MSU channels, channel 2 (53.74 GHz) was the most useful channel in detecting precipitation over land. The brightness temperature values (TB2) of channel 2 alone were not sufficient to detect precipitation; but, a median filter algorithm (MFA2), which isolates precipitation induced decreases in TB2 from the normal background radiative temperature, showed the highest correlations with effective rainfall rate.

The MFA2 value was correlated with Effective Rainfall Rate (ERR) with correlation coefficients of about 0.6 during the spring and summer cases; but during the winter, correlations were near zero.

This study concludes that precipitation is more easily detected over land, with the use of the 53.74 GHz channel 2 via the MFA2 algorithm, during spring and summer when convection is strong (reaching to tropopause levels) and when rain rates are high.

Because of the vertically broad weighting function of MSU Ch 2, which peaks at about the 600 mb level, the MFA2 algorithm should not be used over mountainous areas where heights are above 1500 meters. The 1500-meter elevation flag is currently in use and has been utilized in the TOVS algorithm since 1980.

The present MSU instrument with its low resolution shows no skill in detecting rain rates when they are light. In addition, the algorithm is not reliable when surface elevations exceed 1500 meters; further, it should not be used for those footprints over coastal areas where strong land-water thermal gradients (seabreeze circulations) are suspected to extend higher than one km into the lower atmosphere.

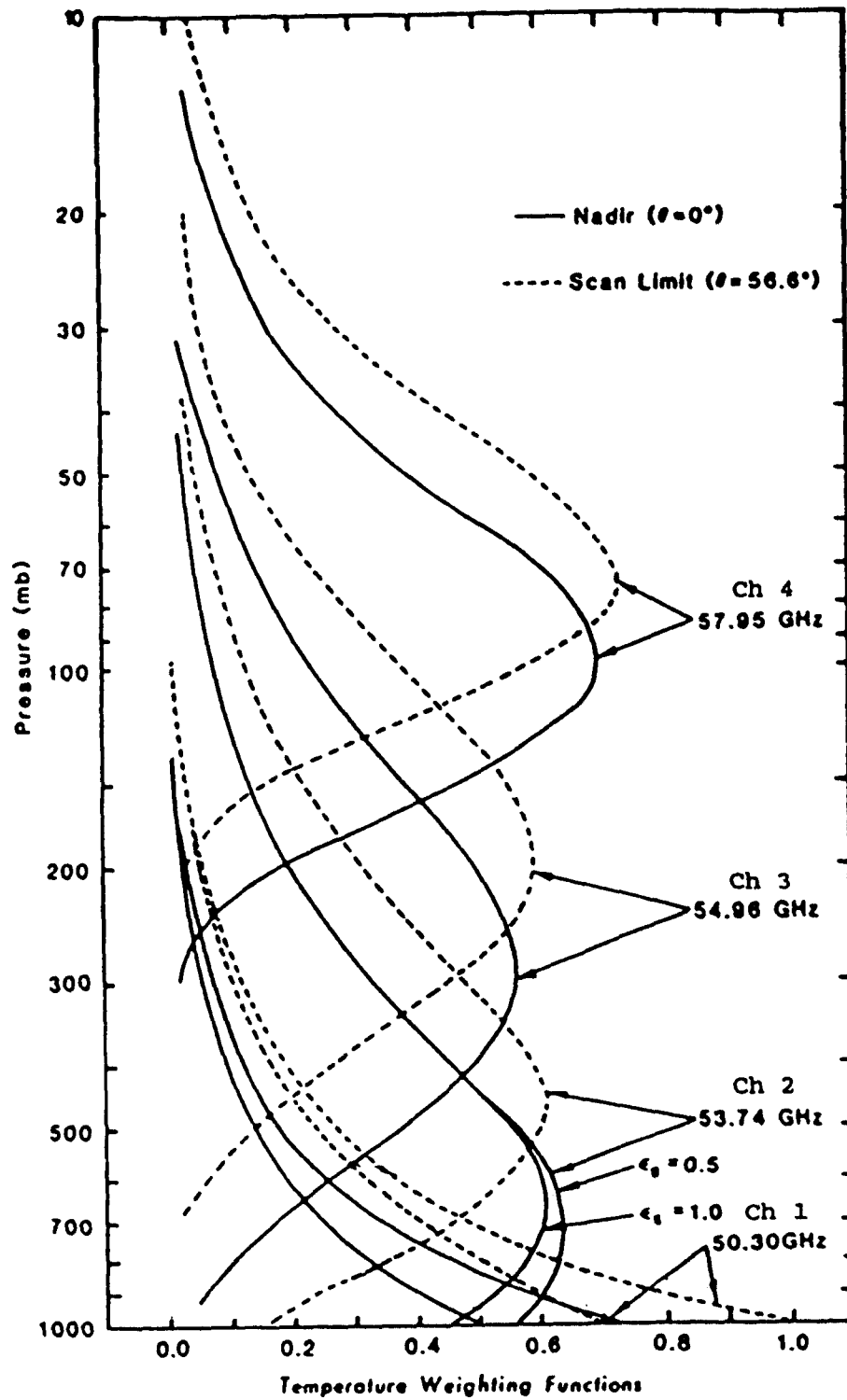


Figure 1. Temperature weighting functions for the four MSU channels for nadir and beam positions #1 and #11 ( $\theta=56.6$  deg). Weighting functions are shown for land ( $\epsilon=1$ ) and sea ( $\epsilon=0.5$ ) type surfaces

-	-	-	-	-	-	-	-	-	-	-
252	252	252	253	252	252	253	253	252	252	253
252	252	252	253	252	252	253	253	253	253	253
252	253	252	253	253	251	254	254	253	254	253
253	253	254	254	253	254	255	255	254	253	254
254	254	255	254	254	254	255	255	255	254	255
-	-	-	-	-	-	-	-	-	-	-

Figure 2. Example of MSU2 brightness temperature (TB2) array used to calculate the Median Filter Anomaly (MFA2)

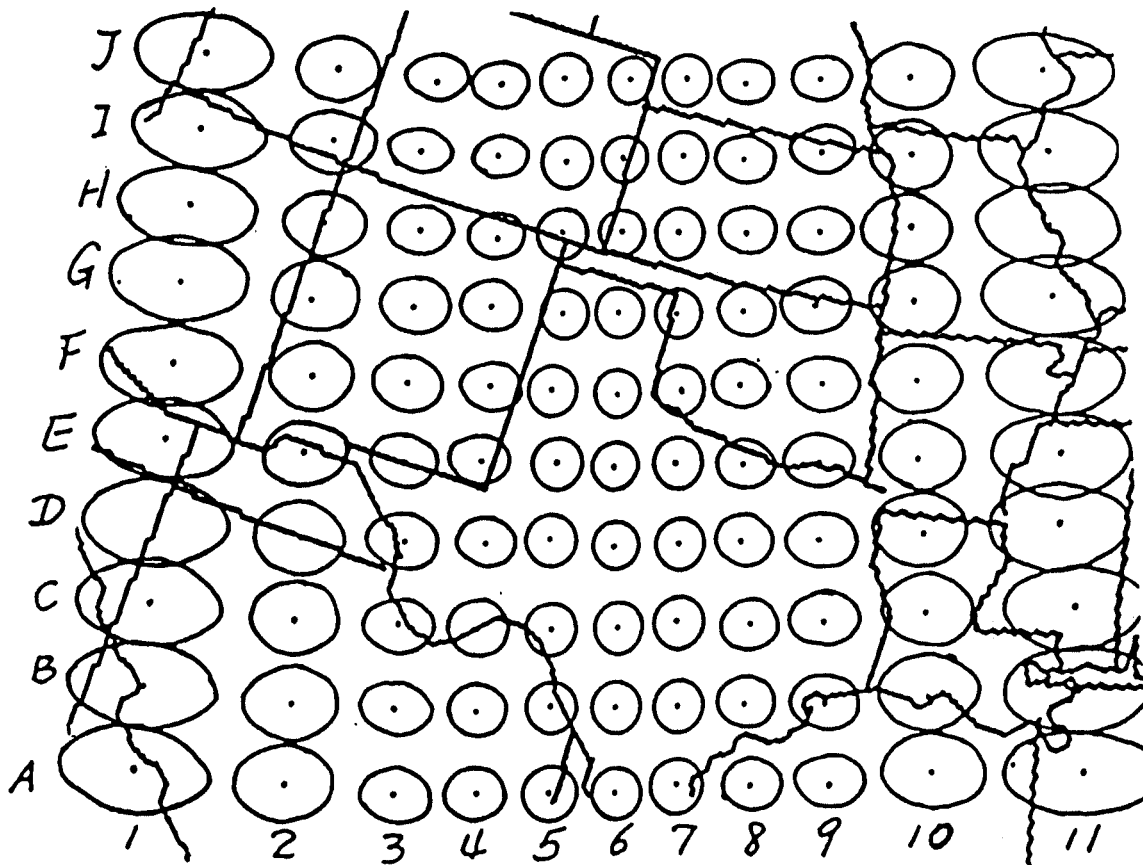


Figure 3a. MSU footprints (IFOV) for 0056 GMT April 8, 1986

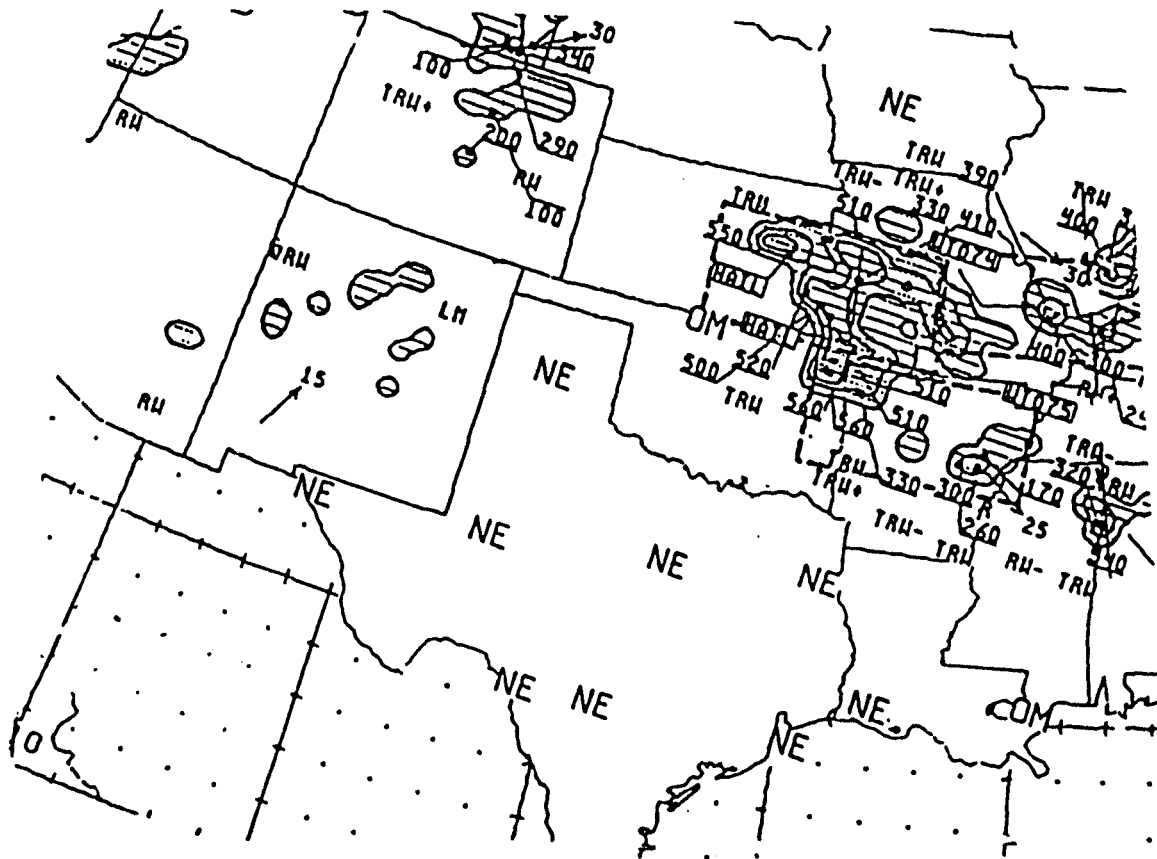


Figure 3b. Radar echo summary chart for 0035 GMT April 8, 1986

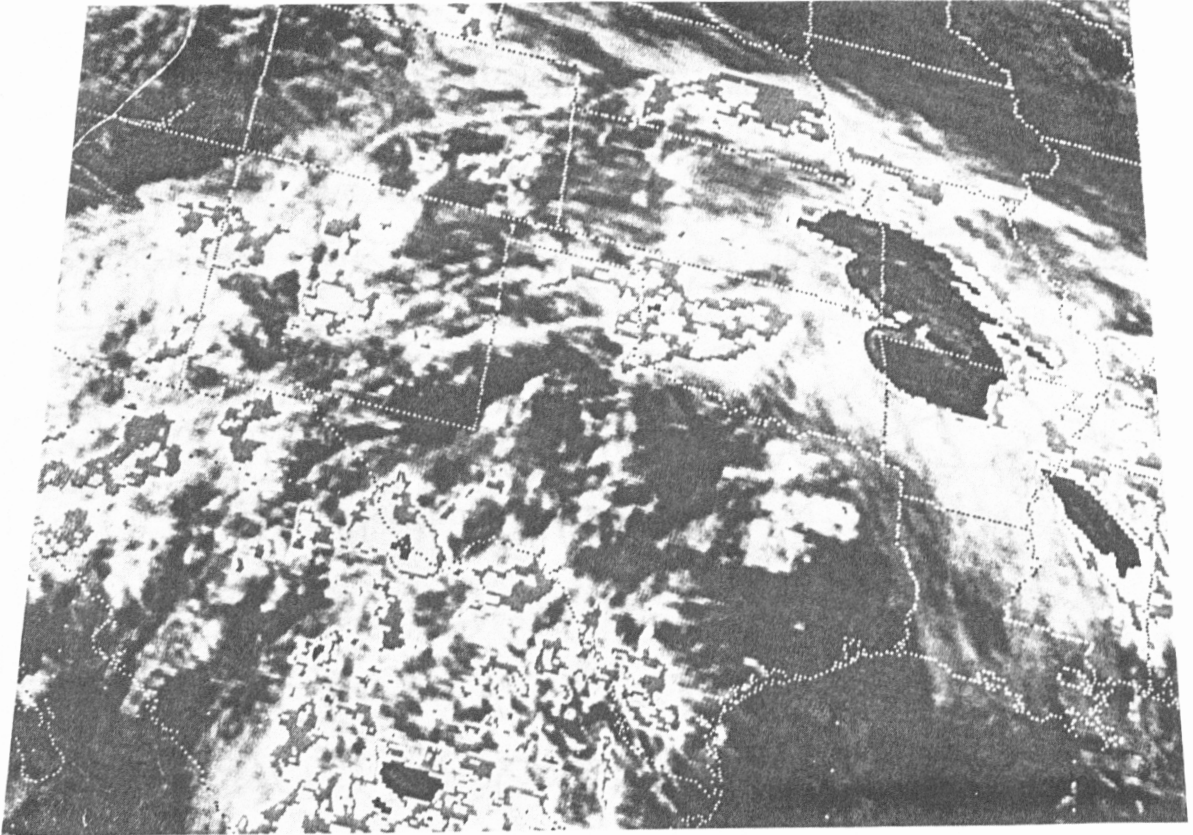


Figure 3c. GOES 6 infrared image 0100 GMT April 8, 1986

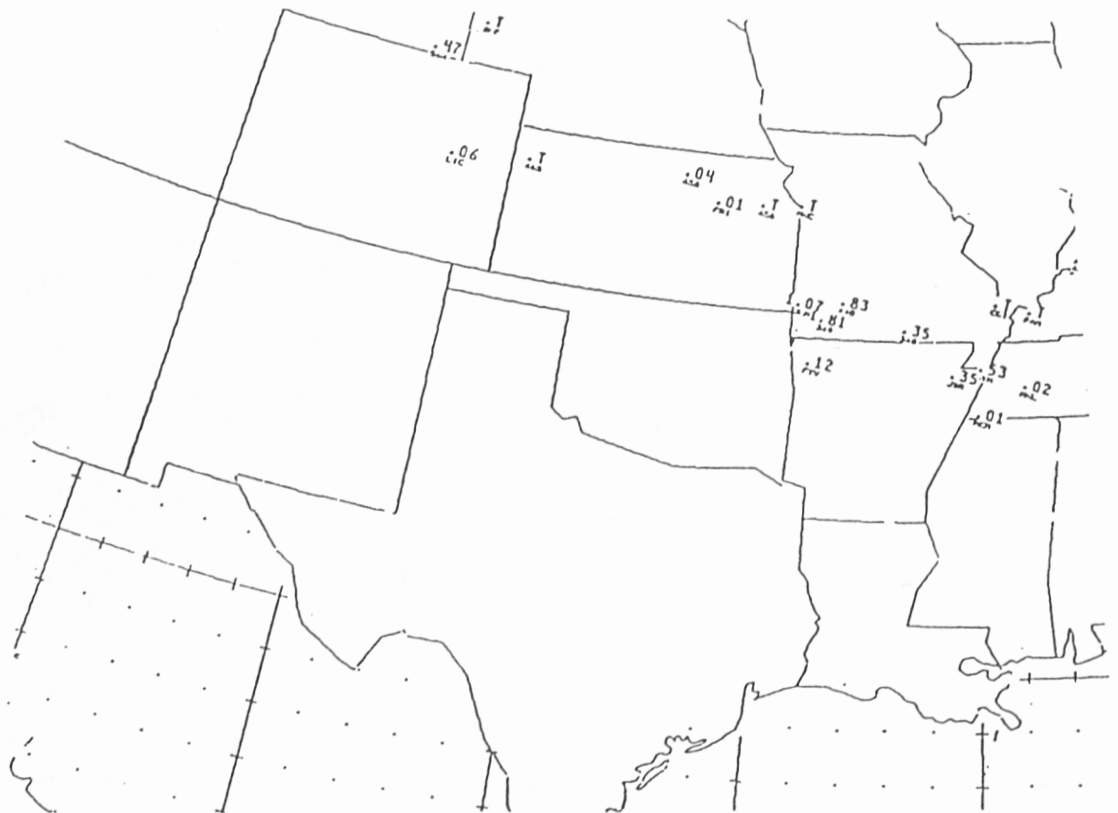


Figure 3d. Six hourly precipitation 06 GMT April 8, 1986

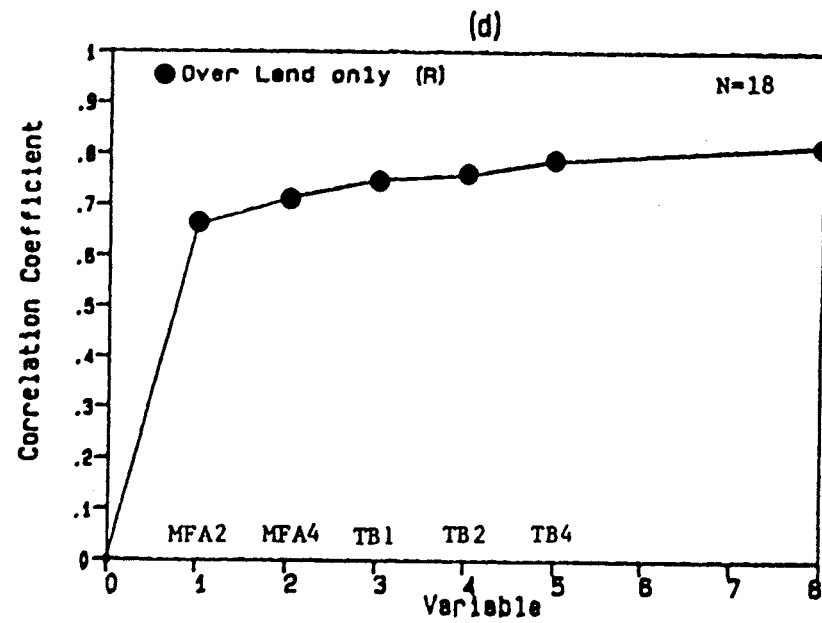
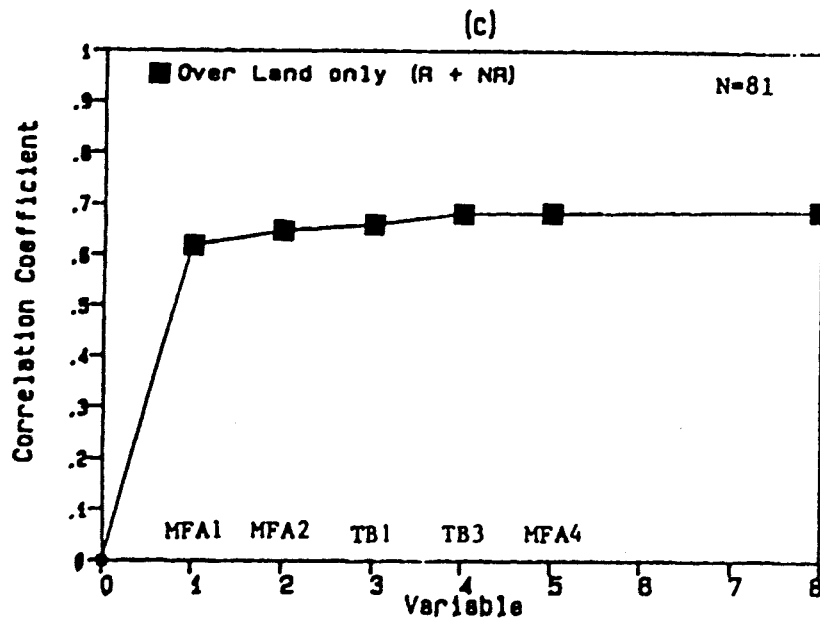
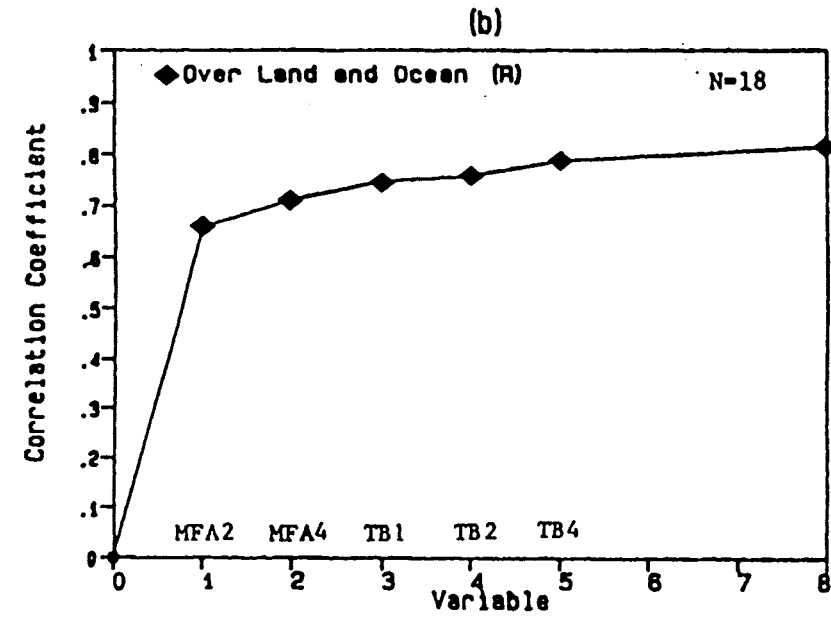
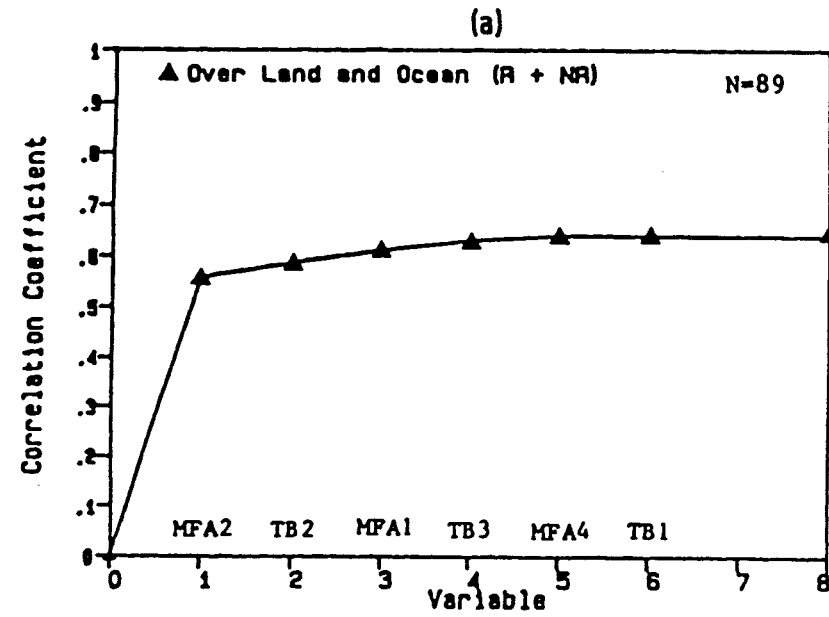


Figure 4. Correlation of Effective Rain Rate (ERR) with MSU variables for 0056 GMT Apr 8, 1986. Abscissa shows order of variable selection using forward stepwise regression method

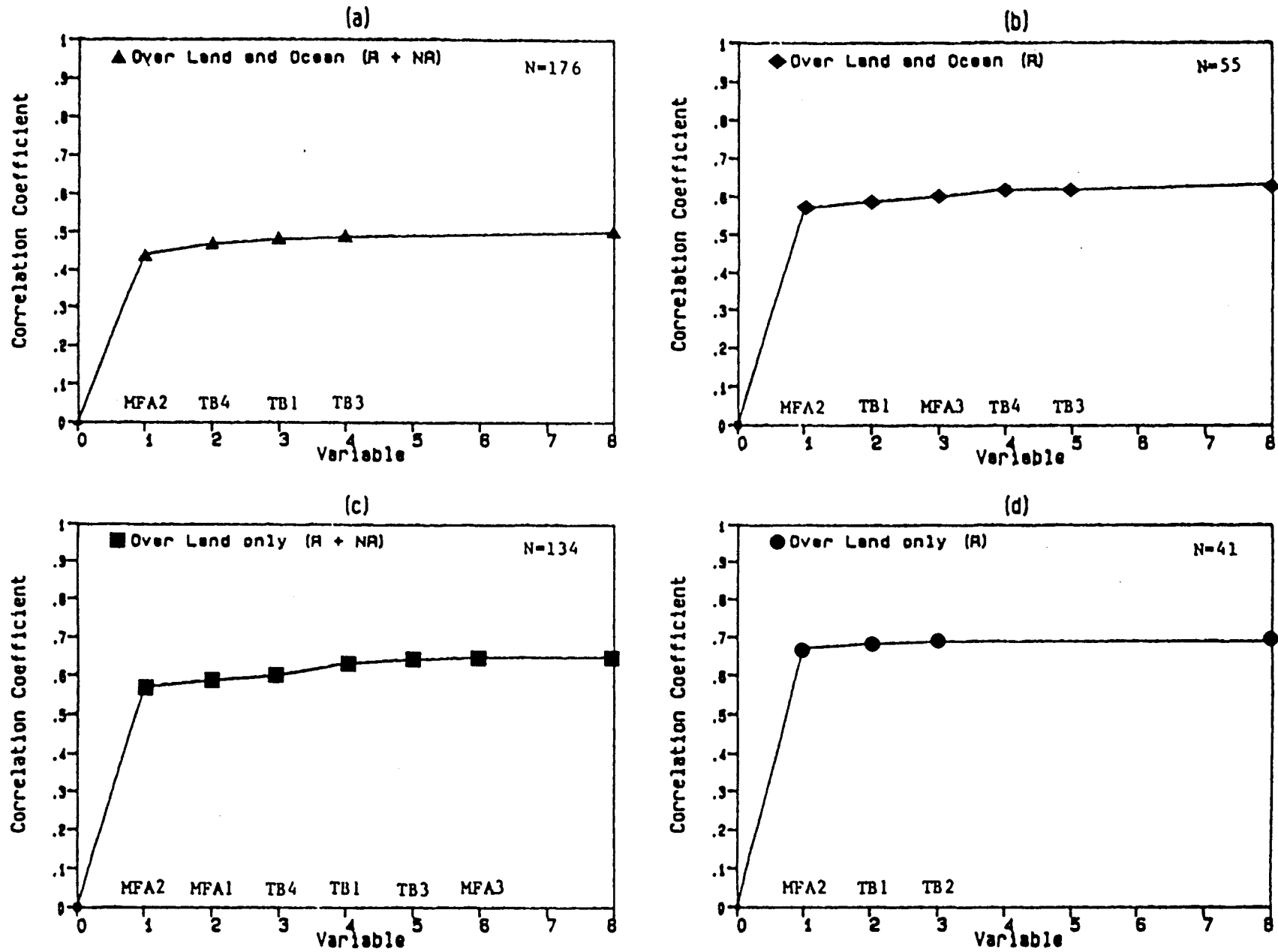


Figure 5. Same as Figure 4 except for 1245 GMT July 1, 1986

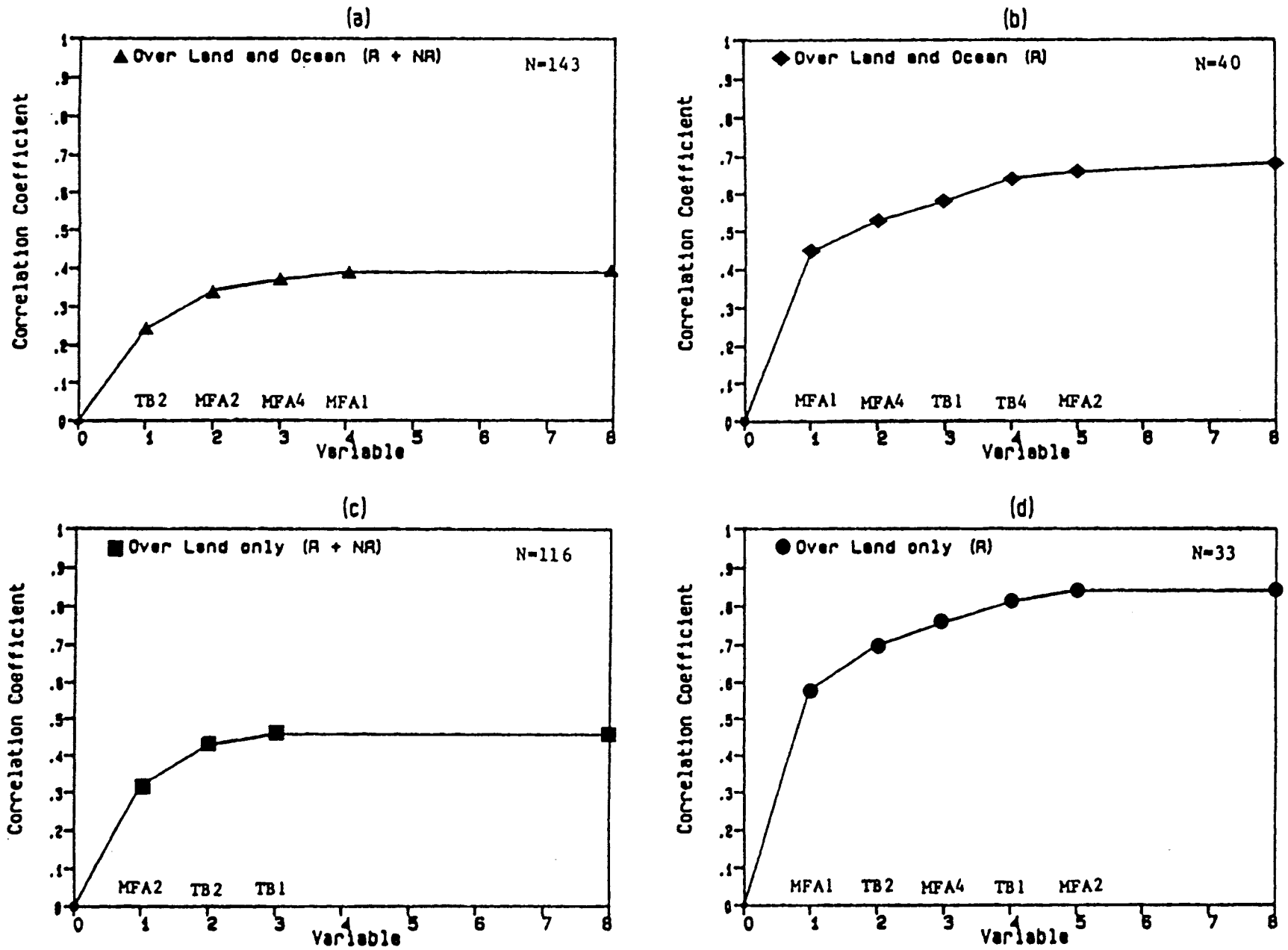


Figure 6. Same as Figure 4 except for 1317 GMT October 24, 1986

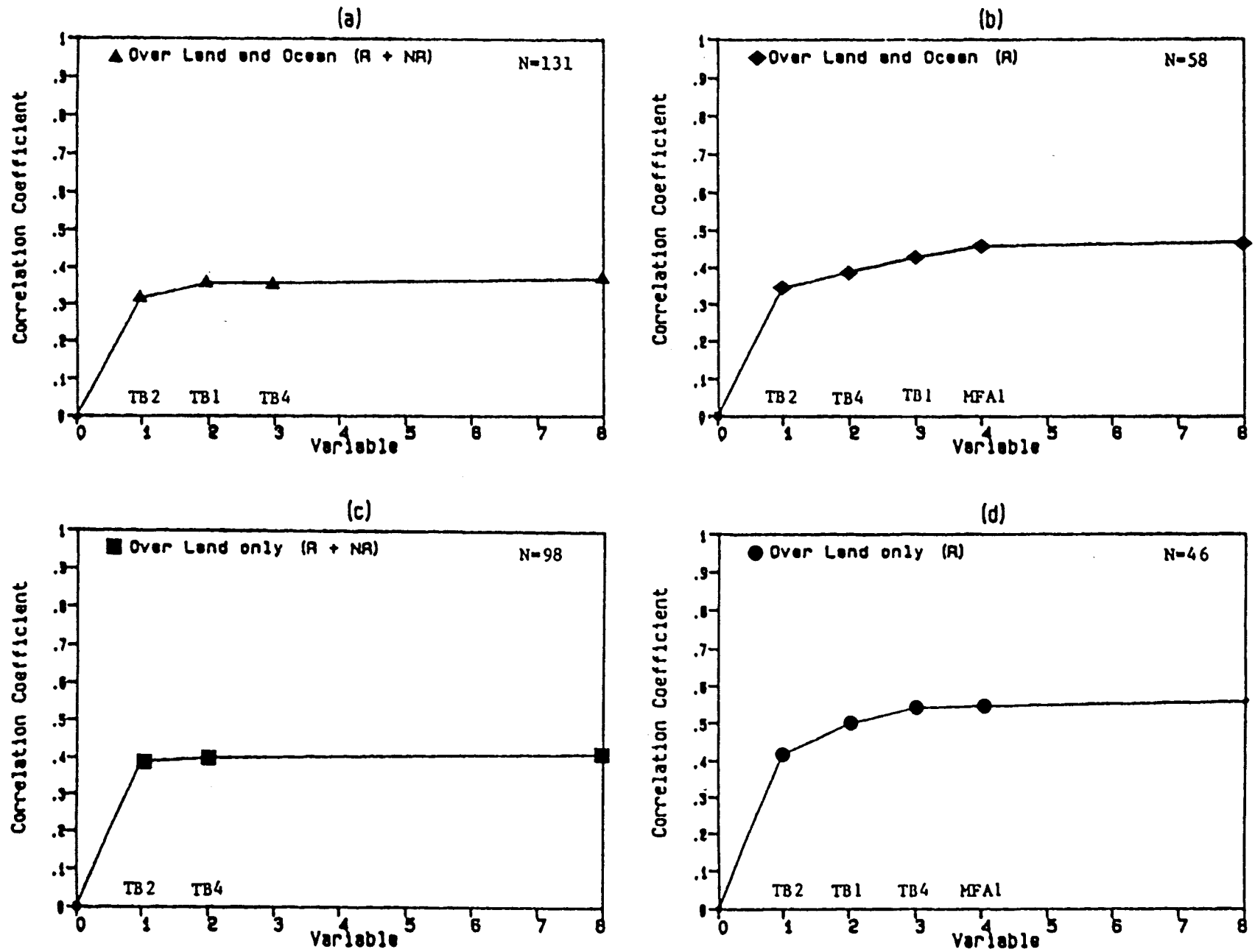


Figure 7. Same as Figure 4 except for 2005 GMT December 9, 1986

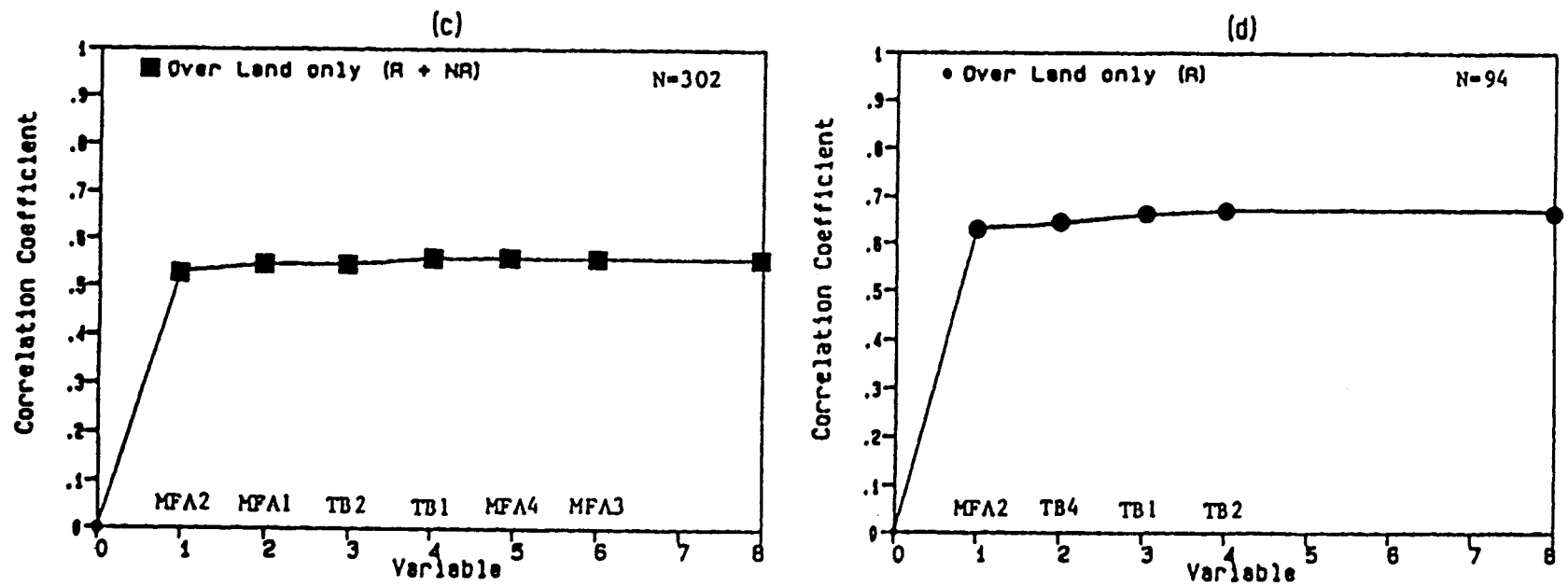


Figure 8. Same as Figure 4 except for April 8, July 1, and October 24, 1986 cases combined (over land only)

Table 1. Radar-echo level (VIP number) conversion to rain rate.

Echo-level (VIP number)	Echo Intensity	Rainfall Rate Convective* (mm/hr)
1	light	2.5
3	heavy	41.9
5	intense	147.3
		1.6

\* Based on the relationship  $Z=55R$

Table 2. Screening regression statistics for ERR as a function of all four MSU TB and MFA values (land only)

Date	4-8-86 0056Z		7-1-86 1245Z		10-24-86 1317Z		12-9-86 2005Z		3 ORBITS	
Sat.	NOAA-6		NOAA-6		NOAA-6		NOAA-9			
	ERR		ERR		ERR		ERR		ERR	
Data	R+NR	R	R+NR	R	R+NR	R	R+NR	R	R+NR	R
n	81	18	105	41	116	33	98	46	302	92
B0	790.47	-2955	-412.8	-79.81	-146.8	-241.0	-156.3	-659.6	-36.89	124.79
B1	-.241	-2.793	-.273	-.184	-.081	-.918	X	-.177	-.098	-.443
B2	X	8.982	X	.517	.672	1.952	.414	1.704	.254	.474
B3	-3.208	X	3.101	X	X	X	X	X	X	X
B4	X	6.836	-1.034	X	X	X	.260	1.346	X	-.574
B5	1.16	X	.02	X	X	1.01	X	-.18	.13	X
B6	2.77	13.41	4.43	6.12	3.62	3.05	X	X	4.94	6.60
B7	X	X	2.19	X	X	X	X	X	1.00	X
B8	5.39	39.70	X	X	X	-9.86	X	X	1.23	X
r	.68**	.79	.65**	.69**	.46**	.84**	.40**	.55**	.56**	.67**
S	6.38	12.22	3.48	4.77	3.07	3.50	2.94	3.62	4.60	7.03
ERR(AV)	1.77	7.96	1.65	4.22	0.90	3.15	1.36	2.89	1.39	4.57
TB2(AV)	254.9	252.7	258.1	258.2	251.8	252.1	248.8	251.9	254.8	254.9

ERR (mm/hr) = B0 + B1(TB1) + B2(TB2) + B3(TB3) + B4(TB4) + B5(MFA1) + B6(MFA2) + B7(MFA3) + B8(MFA4)

NOTE: X = Not selected by stepwise regression  
 \* = Significant 5% level  
 \*\* = Significant 1% level  
 R = Rain  
 NR = No rain



Table 5. Distribution of Ch 2 Median Filter Anomaly (MFA2) as a function of Effective Rain Rate (ERR) for 0056 GMT April 8, 1986.

MFA2	n	< -1.0	-1.0 to -0.5	-0.5 to 0.0	0.0 to 0.5	0.5 to 1.0	1.0 to 1.5	1.5 to 2.0	> 2.0	
HEAVY F(%)	3 100%	0 0%	0 0%	0 0%	0 0%	0 0%	0 0%	1 33%	2 67%	
MODERATE F(%)	2 100%	0 0%	0 0%	1 50%	0 0%	0 0%	0 0%	0 0%	1 50%	
LIGHT F(%)	13 100%	2 15%	0 0%	3 23%	4 31%	1 8%	3 23%	0 0%	0 0%	
NORAIN F(%)	63 100%	4 6%	6 10%	18 29%	18 29%	13 21%	2 3%	1# 1%	1* 1%	0 0%
SUM(n) F(%)	81 100%	6 7%	6 7%	22 27%	22 28%	14 17%	5 6%	1 1%	2 3%	3 4%

Table 6. Distribution of Ch 2 Median Filter Anomaly (MFA2) as a function of Effective Rain Rate (ERR) for 1245 GMT July 1, 1986.

MFA2	n	< -1.0	-1.0 to -0.5	-0.5 to 0.0	0.0 to 0.5	0.5 to 1.0	1.0 to 1.5	1.5 to 2.0	> 2.0
HEAVY F(%)	9 100%	0 0%	0 0%	0 0%	0 0%	5 56%	3 33%	0 0%	1 11%
MODERATE F(%)	6 100%	0 0%	1 17%	1 17%	1 17%	0 0%	1 16%	0 0%	1 16%
LIGHT F(%)	26 100%	0 0%	4 16%	11 42%	6 23%	5 19%	0 0%	0 0%	0 0%
NORAIN F(%)	64 100%	3 5%	2 3%	19 30%	26 40%	12 19%	2 3%	0 0%	0 0%
SUM(n) F(%)	105 100%	3 3%	7 7%	31 29%	33 31%	18 17%	7 7%	4 4%	0 0%

Table 7. Distribution of Ch 2 Median Filter Anomaly (MFA2) as a function of Effective Rain Rate (ERR) for 1317 GMT October 24, 1986.

MFA2	n	< -1.0	-1.0 to -0.5	-0.5 to 0.0	0.0 to 0.5	0.5 to 1.0	1.0 to 1.5	1.5 to 2.0	> 2.0
HEAVY F(%)	4 100%	0 0%	0 0%	1 25%	1 25%	1 25%	0 0%	0 0%	1 25%
MODERATE F(%)	4 100%	0 0%	1 25%	1 25%	0 0%	1 25%	0 0%	1 25%	0 0%
LIGHT F(%)	25 100%	0 0%	4 16%	4 16%	8 32%	8 32%	1 4%	0 0%	0 0%
NORAIN F(%)	83 100%	1 1%	4 5%	22 26%	30 36%	23 28%	3 4%	0 0%	0 0%
SUM(n) F(%)	116 100%	1 1%	9 8%	28 24%	39 34%	33 28%	4 3%	1 1%	0 0%

Table 8. Distribution of Ch 2 Median Filter Anomaly (MFA2) as a function of Effective Rain Rate (ERR) for 2005 GMT December 5, 1986.

MFA2	n	< -1.0	-1.0 to -0.5	-0.5 to 0.0	0.0 to 0.5	0.5 to 1.0	1.0 to 1.5	1.5 to 2.0	> 2.0
HEAVY F(%)	5 100%	0 0%	0 0%	2 40%	2 40%	1 20%	0 0%	0 0%	0 0%
MODERATE F(%)	5 100%	0 0%	0 0%	0 0%	4 80%	1 20%	0 0%	0 0%	0 0%
HEAVY F(%)	36 100%	0 0%	1 3%	4 11%	24 67%	7 19%	0 0%	0 0%	0 0%
NORAIN F(%)	52 100%	0 0%	2 4%	10 19%	27 52%	13 25%	0 0%	0 0%	0 0%
SUM(n) F(%)	98 100%	0 0%	3 3%	16 16%	57 58%	22 23%	0 0%	0 0%	0 0%

Table 9. Distribution of Ch 2 Median Filter Anomaly (MFA2) as a function of Effective Rain Rate (ERR) for April, July, and October, 1986 cases combined.

MFA2	n	< -1.0	-1.0 to -0.5	-0.5 to 0.0	0.0 to 0.5	0.5 to 1.0	1.0 to 1.5	1.5 to 2.0	> 2.0	
HEAVY F(%)	16 100%	0 0%	0 0%	1 6%	1 6%	1 6%	5 31%	3 19%	1 7%	4 25%
MODERATE F(%)	12 100%	0 0%	2 17%	3 25%	1 8%	2 17%	0 0%	2 17%	0 0%	2 16%
LIGHT F(%)	64 100%	2 3%	8 13%	18 28%	18 28%	14 22%	4 6%	0 0%	0 0%	0 0%
NORAIN F(%)	210 100%	8 4%	12 6%	59 28%	74 35%	48 22%	7 3%	1# 1%	1* 1%	0 0%
SUM(n) F(%)	302 100%	10 3%	22 7%	80 27%	94 31%	65 22%	16 5%	6 2%	2 1%	6 2%

Table 10. Distribution of Ch 2 Median Filter Anomaly (MFA2) as a function of Effective Rain Rate (ERR) for April, July, October, and December cases combined.

MFA2	n	< -1.0	-1.0 to -0.5	-0.5 to 0.0	0.0 to 0.5	0.5 to 1.0	1.0 to 1.5	1.5 to 2.0	> 2.0	
HEAVY F(%)	21 100%	0 0%	0 0%	3 14%	3 14%	2 10%	5 24%	3 14%	1 5%	4 19%
MODERATE F(%)	17 100%	0 0%	2 12%	3 18%	5 29%	3 18%	0 0%	2 12%	0 0%	2 11%
LIGHT F(%)	100 100%	2 2%	9 9%	22 22%	42 42%	21 21%	4 4%	0 0%	0 0%	0 0%
NORAIN F(%)	262 100%	8 3%	14 5%	69 26%	101 38%	61 23%	7 3%	1# 1%	1* 1%	0 0%
SUM(n) F(%)	400 100%	10 3%	25 6%	97 24%	151 38%	87 22%	16 4%	6 1%	2 1%	6 1%

Table 11. Effective Rain Rate (ERR) values regressed on Ch 2 Median Filter Anomaly (MFA2) values for each ERR class. Samples are for April, July, and October, 1986 cases combined.

ERR CLASS mm/hr	N	A	B	r	S	ERR (ave)	TB2 (ave)
LIGHT 0 -2.53	64	.63	-.06	-.04	.58	.63	254.7
MODERATE 2.54-7.62	12	4.26	.55	.30	1.72	4.51	255.6
HEAVY >7.62	16	13.47	5.80	.45	12.50	20.4	255.4

(Continued from inside front cover)

- NESDIS 16 Temporal and Spatial Analyses of Civil Marine Satellite Requirements. Nancy J. Hooper and John W. Sherman III, February 1985. (PB86 212123/AS)
- NESDIS 17 reserved
- NESDIS 18 Earth Observations and the Polar Platform. John H. McElroy and Stanley R. Schneider, January 1985. (PB85 177624/AS)
- NESDIS 19 The Space Station Polar Platform: Intergrating Research and Operational Missions. John H. McElroy and Stanley R. Schneider, January 1985. (PB85 195279/AS)
- NESDIS 20 An Atlas of High Altitude Aircraft Measured Radiance of White Sands, New Mexico, in the 450-1050nm Band. Gilbert R. Smith, Robert H. Levin and John S. Knoll, April 1985. (PB85 204501/AS)
- NESDIS 21 High Altitude Measured Radiance of White Sands, New Mexico, in the 400-2000nm Band Using a Filter Wedge Spectrometer. Gilbert R. Smith and Robert H. Levin, April 1985. (PB85 206084/AS)
- NESDIS 22 The Space Station Polar Platform: NOAA Systems Considerations and Requirements. John H. McElroy and Stanley R. Schneider, June 1985. (PB86 6109246/AS)
- NESDIS 23 The Use of TOMS Data in Evaluating and Improving the Total Ozone from TOVS Measurements. James H. Lienesch and Prabhat K.K. Pandey, July 1985. (PB86 108412/AS)
- NESDIS 24 Satellite-Derived Moisture Profiles. Andrew Timchalk, April 1986. (PB86 232923/AS)
- NESDIS 25 reserved
- NESDIS 26 Monthly and Seasonal Mean Outgoing Longwave Radiation and Anomalies. Arnold Gruber, Marylin Varnadore, Phillip A. Arkin, and Jay S. Winston, October 1987. (PB87160545/AS)
- NESDIS 27 Estimation of Broadband Planetary Albedo from Operational Narrowband Satellite Measurements. James Wydick, April 1987. (PB88-107644/AS)
- NESDIS 28 The AVHRR/HIRS Operational Method for Satellite Based Sea Surface Temperature Determination. Charles Walton, March 1987. (PB88-107594/AS)
- NESDIS 29 The Complementary Roles of Microwave and Infrared Instruments in Atmospheric Sounding. Larry McMillin, February 1987. (PB87 184917/AS)
- NESDIS 30 Planning for Future Generational Sensors and Other Priorities. James C. Fischer, June 1987. (PB87 220802/AS)
- NESDIS 31 Data Processing Algorithms for Inferring Stratospheric Gas Concentrations from Balloon-Based Solar Occultation Data. I-Lok Chang (American University) and Michael P. Weinreb, April 1987. (PB87 196424)
- NESDIS 32 Precipitation Detection with Satellite Microwave Data. Yang Chenggang and Andrew Timchalk, June 1988, 27 pp.
- NESDIS 33 An Introduction to the GOES I-M Imager and Sounder Instruments and the GVAR Retransmission Format. Raymond J. Komajda (Mitre Corp) and Keith McKenzie, October 1987, 47 pp.
- NESDIS 34 Balloon-Based Infrared Solar Occultation Measurements of Stratospheric O<sub>3</sub>, H<sub>2</sub>O, HNO<sub>3</sub>, and CF<sub>2</sub>C<sub>12</sub>. Michael P. Weinreb and I-Lok Chang (American University), September 1987, 27 pp.
- NESDIS 35 Passive Microwave Observing From Environmental Satellites, A Status Report Based on NOAA's June 1-4, 1987, Conference in Williamsburg, Virginia. James C. Fischer, November 1987. (PB88-208236)
- NESDIS 36 Pre-Launch Calibration of Channels 1 and 2 of the Advanced Very High Resolution Radiometer. C.R. Nagaraja Rao, October 1987.
- NESDIS 39 General Determination of Earth Surface Type and Cloud Amount Using Multispectral AVHRR Data. Irwin Ruff and Arnold Gruber, February 1988. (PB88-199195/AS)

## NOAA SCIENTIFIC AND TECHNICAL PUBLICATIONS

*The National Oceanic and Atmospheric Administration* was established as part of the Department of Commerce on October 3, 1970. The mission responsibilities of NOAA are to assess the socioeconomic impact of natural and technological changes in the environment and to monitor and predict the state of Earth, the oceans and their living resources, the atmosphere, and the space environment of the Earth.

The major components of NOAA regularly produce various types of scientific and technical publications in the following kinds of publications:

**PROFESSIONAL PAPERS**—Important definitive research results, major techniques, and special investigations.

**CONTRACT AND GRANT REPORTS**—Reports prepared by contractors or grantees under NOAA sponsorship.

**ATLAS**—Presentation of analyzed data generally in the form of maps showing distribution of rainfall, chemical and physical conditions of oceans and atmosphere, distribution of fishes and marine mammals, ionospheric conditions, etc.

**TECHNICAL SERVICE PUBLICATIONS**—Reports containing data, observations, instructions, etc. A partial listing includes data serials; prediction and outlook periodicals; technical manuals, training papers, planning reports, and information serials; and miscellaneous technical publications.

**TECHNICAL REPORTS**—Journal quality with extensive details, mathematical developments, or data listings.

**TECHNICAL MEMORANDUMS**—Reports of preliminary, partial, or negative research or technology results, interim instructions, and the like.



Stimulating America's Progress  
1913-1988

U.S. DEPARTMENT OF COMMERCE  
NATIONAL OCEANIC AND ATMOSPHERIC ADMINISTRATION  
NATIONAL ENVIRONMENTAL SATELLITE, DATA, AND INFORMATION SERVICE  
Washington, D.C. 20233

